Research Article

Nano Research
2024, 17(6): 4986–4993

ISSN 1998-0124 CN 11-5974/O4
https://doi.org/10.1007/s12274-024-6508-6

Geometric edge effect on the interface of Au/CeO_2 nanocatalysts for CO oxidation

Hongpeng Liu[1,§], Zhongliang Cao[1,§], Siyuan Yang[1,§], Qingye Ren[1], Zejian Dong[1], Wei Liu[2], Zi-An Li[3] (✉), Xing Chen[1,4] (✉), and Langli Luo[1,4] (✉)

[1] *Institute of Molecular Plus, Tianjin University, Tianjin 300072, China*
[2] *Dalian National Laboratory for Clean Energy, Dalian Institute of Chemical Physics (DICP), Chinese Academy of Sciences, Dalian 116023, China*
[3] *State Key Laboratory of Featured Metal Materials and Life-cycle Safety for Composite Structures, and School of Physical Science and Technology, Guangxi University, Nanning 530004, China*
[4] *Haihe Laboratory of Sustainable Chemical Transformations, Tianjin 300192, China*
[§] *Hongpeng Liu, Zhongliang Cao, and Siyuan Yang contributed equally to this work.*

Received: 17 November 2023 / **Revised:** 6 January 2024 / **Accepted:** 21 January 2024

ABSTRACT

The oxide supports play a crucial role in anchoring and promoting the active metal species by geometric confinement and chemical interaction. The design and synthesis of the well-defined oxide support with specific morphology such as size, shape, and exposed facets have attracted extensive research efforts, which directly reflects on their catalytic performance. In this study, using an Au/CeO_2-nanorod model catalyst, we demonstrate an edge effect on the Au/CeO_2 interfacial structure, which shows a prominent effect on the structure–performance relationship in the CO oxidation reaction. This specific "edge-interface" structure features an "edge-on" Au nanoparticles position on rod-shaped CeO_2 support, confirmed by atomic-scale electron microscopy characterization, which introduces additional degrees of freedom in coordination environment, chemical state, bond length, and strength. Combined with theocratical calculations and *in situ* diffuse reflectance infrared Fourier transform spectroscopy (DRIFTS) investigations, we confirmed that this "edge-interface" has distinct adsorption properties due to the change of O vacancy formation energy as well as the chemical states of Au resulting from the electron transfer and redistribution between the metal and the support. These results demonstrate a non-conventional geometric effect of rod-shaped supported metal catalysts on the catalytic performance, which could provide insights into the atomic-precise utilization of catalysts.

KEYWORDS

ceria, nanorod, supported catalyst, edge-effect, atomic scale

1 Introduction

Metallic nanoparticles supported on oxides prevail in the field of heterogeneous catalysis due to their fine dispersion and stable anchoring of metal species [1–6]. Oxide supports, especially reducible oxides (e.g., CeO_2 and TiO_2), can participate in the chemical reactions through the O shuttling process and metal–support interaction, which have a significant impact on the catalytic performance [7–10]. The metal–oxide interface plays a crucial role in determining the structure–property relationship of supported metal catalysts, and it often acts as the active site for chemical reactions [11–15]. Hence, it is of great importance to tune the interface between metal species and oxide support to achieve superior activity, selectivity, and stability. The identification of exact interfacial structure becomes a prerequisite but remains challenging because of its buried nature, where most characterization techniques fall short of getting helpful information.

CeO_2 is an extensively investigated reducible oxide support due to its exceptional oxygen storage capacity and varied oxidation states by forming a large number of oxygen vacancies (OVs) [16–20]. It exhibits excellent performance in many catalytic reactions, such as CO-oxidation [21–24], preferential-CO-oxidation under reducing atmospheres (PROX) [25–27], and the water–gas shift (WGS) reaction [28–32]. The formation of oxygen vacancies in CeO_2 is strongly correlated with crystal facets through theoretical calculations, indicating that its properties are highly sensitive to its morphology and microstructure [33–40]. Three typical morphologies of CeO_2 support are nanocube, octahedra, and nanorods [41–45], which provide a convenient model catalyst system to assess the facet-dependent catalytic properties since only (100) and (111) crystal planes are found on cube and octahedron CeO_2 supports, respectively [13]. Meanwhile, CeO_2 nanorods often expose a combination of low-indexed crystal planes [35, 37–39]. For instance, Li et al. compared CeO_2 nanocubes, octahedra, and four-sided nanorods exposing two (100) facets and two (110) facets, where the nanorods exhibited the best reactivity in CO oxidation due to the exposure of more (110) facets [39]. Subsequent research on the catalytic performance of CeO_2-supported catalysts for CO oxidation [44] and the WGS reaction [46] agreed with the above conclusion, which seems to match with the theoretical calculations of the formation energies of oxygen vacancies and different CO adsorption abilities for the three crystal facets: (110) > (100) > (111) [47, 48].

Address correspondence to Zi-An Li, zianli@gxu.edu.cn; Xing Chen, xing_chen@tju.edu.cn; Langli Luo, luolangli@tju.edu.cn

清華大學出版社 Tsinghua University Press Springer

However, CeO_2 nanorods with a hexagonal cross-sectional shape exposing two (100) and four (111) facets have been reported to have superior catalytic performance than the four-sided nanorods, despite the absence of (110) facets [49]. Actually, all CeO_2 nanorods (rectangle, pentagonal, and hexagonal) show better catalytic performance than that of other morphologies, e.g., cubic and octahedron when used alone [37, 38] or as catalyst supports [39, 45, 49–51]. Hence, we suspect that there may be factors, apart from the facets of the CeO_2 nanorods, to strongly influence their performance. Herein, we synthesized Au nanoparticles supported on CeO_2 nanorods as the model catalysts and conducted detailed structural characterizations by transmission electron microscopy (TEM) to identify the geometry of Au nanoparticles with respect to the CeO_2 nanorods. We found that the majority of Au nanoparticles have preferred sites on the CeO_2 nanorods, i.e., located at the edges of CeO_2 nanorods. This specific structure relationship between Au and CeO_2 partially exposes the interface as a surface of the whole materials system. Through density functional theory (DFT) calculations, we found that these sites have a lower formation energy for oxygen vacancies and higher adsorption energy. *In situ* diffuse reflectance infrared Fourier transform spectroscopy (DRIFTS) confirmed that these edge sites show distinct adsorption behaviors of CO molecules. We also used X-ray photoelectron spectroscopy (XPS) to validate the occurrence of electron transfer at these edge sites, which is distinct from the inner region of the general crystal plane. All of the above results demonstrated that the "edge interface" of Au/CeO_2 has a strong influence on the catalytic performance for CO oxidation, which could be extrapolated to other supported metal catalysts.

2 Results and discussion

2.1 Geometric structure of Au nanoparticles on CeO_2

Using a hydrothermal method [45], we synthesized ceria supports with three different morphologies: ceria cube (CeO_2-C) exposing six (100) facets, ceria octahedra (CeO_2-O) with eight (111) facets, and one-dimensional ceria rods (CeO_2-R). As the final step of ceria preparation, the samples were air-calcined at 500 °C for 2 h to ensure surface purity without hydroxyl groups. Subsequently, Au nanoparticles (Au NPs) were deposited onto the CeO_2 supports using a deposition–precipitation method (details in the Electronic Supplementary Material (ESM)) [52]. Through the X-ray diffraction (XRD) (Fig. S1 in the ESM) and energy-dispersive X-ray spectroscopy (EDS) elemental mapping (Fig. S2 in the ESM), we can confirm the successful synthesis of three target Au/CeO_2 catalysts. The overall morphology of the Au/CeO_2 catalysts is depicted in Figs. 1(a)–1(c) by high-angle annular dark field (HAADF), also seen in Fig. S3 in the ESM. For the octahedra Au/CeO_2 catalysts (Au/CeO_2-O) sample (Fig. 1(a)), it can be observed that the lateral size of CeO_2 octahedron is ~ 100 nm, and the average size of Au nanoparticles loaded on the CeO_2-O is 7.3 ± 2 nm (Fig. 1(d)). In contrast, the sizes of CeO_2-C in the cube Au/CeO_2 catalysts (Au/CeO_2-C) range between 30 and 50 nm, and the average size of Au nanoparticles loaded on it (3.4 ± 1.2 nm) is much smaller than that on the CeO_2-O (Fig. 1(e)). It should be emphasized that the conditions for loading Au nanoparticles were identical for all three substrates, thus the difference in particle size can be directly correlated to the effect of surface crystal planes of CeO_2. Studies have shown that the binding of Au nanoparticles to the CeO_2(100) surface is much stronger compared with the (111) surface [34] and is also more prone to forming O vacancies [13], both of which promote the anchoring of Au. Both of above factors contribute to the inhibition of Au growth, leading to smaller particle sizes on the CeO_2(100) facet.

However, the distribution of Au nanoparticles on the rod-shaped Au/CeO_2 catalysts (Au/CeO_2-R) substrate does not follow a simple surface effect. Determination of the actual shape of CeO_2 nanorods and exposed crystal facets is a pre-requisite, which often relies on detailed structure characterization and analysis by TEM. We identified that the morphology of our CeO_2 nanorods has a cross-sectional shape of hexagonal prism with four (111) facets and two (100) facets supported by the following two pieces of evidence. Firstly, we successfully obtained high-resolution TEM (HRTEM) images of the cross-section of the CeO_2 nanorods, as shown in Fig. 1(g) (more examples and HAADF image are shown in Fig. S4 in the ESM), which shows a non-regular hexagon formed by (111) facets (with a lattice spacing of 3.1 Å) and (100) facets (with a lattice spacing of 2.7 Å) surrounded by an angle of 125.3°. Secondly, we imaged the Au-CeO_2 interface through an exact "edge-on" viewing direction, as shown in Figs. 1(h) and 1(i). It is noted that since TEM images are two-dimensional projections of three-dimensional objects, the cross-sectional projection of the metal–oxide interface should be only a line without any interference contrast between the Au nanoparticle and the CeO_2 substrate (detailed geometric analysis is shown in Fig. S5 in the ESM). Therefore, above results confirm the presence of (111) and (100) facets as two exposed surfaces of the CeO_2-R, which grows a hexagonal prism along the (110) direction enclosed by two (100) and four (111) facets. Based on the above analysis, we can confirm that the ceria rod we synthesized has the same hexagonal-prism shape that has been researched in these previous reports [34, 49], and the atomic models of the Au/CeO_2-R are depicted in Figs. 1(j) and 1(k).

Then, we evaluated the catalytic performance of three model Au/CeO_2 catalysts for CO oxidation and revealed that, consistent with previous literature reports [44], Au/CeO_2-R showed much better performance (in terms of the lowest temperature for 100% CO conversion) compared with Au/CeO_2-C and Au/CeO_2-O, as shown in Fig. 2(a). However, this contradicts the conventional explanation of the boosted catalytic performance of CeO_2-R, since our CeO_2-R does not contain any (110) facets, which is believed to be critical to enhance the performance of Au/CeO_2 for CO oxidation reaction. It is noted that the Au size is comparable for Au/CeO_2-R (3.3 ± 0.7 nm) and Au/CeO_2-C (3.4 ± 1.2 nm), as shown in Figs. 1(e) and 1(f). Hence, a combination of (100) and (111) facets of CeO_2-R shows much superior catalytic property than both pure (100) and (111) facets on CeO_2-C and CeO_2-O, respectively. In order to completely eliminate the effect of size-effect, we also used pre-synthesized Au nanoparticles physically loaded on the supports, obtained the three Au/CeO_2 catalysts with completely consistent Au particle size, and still obtained the best performance result of Au/CeO_2-R catalyst, as shown in Fig. S6 in the ESM. Apparently, the difference in crystal plane alone is insufficient to accurately explain this anomalous behavior.

Through extensive and detailed structure analysis, we find that the interface between Au nanoparticles and CeO_2 support holds the key for the varied catalytic performance. Figures 2(b) and 2(c) show that for the Au/CeO_2-C and Au/CeO_2-O catalysts, a large number of Au NPs are scattered within the planar surface, and the number of NPs that can be found on the edges of the CeO_2-C or CeO_2-O is negligible. But for the Au/CeO_2-R catalyst, because of its high aspect ratio, its small axial size (~ 7.6 ± 1.5 nm) leads to limited widths (2–5 nm) of surface facets of the hexagonal prism, e.g., the (100) facet is ~ 3.8 nm, and the (111) facet is ~ 2.8 nm for a common case. This certainly imposes a geometric confinement on the Au nanoparticles loaded on since the cross-edge growth of

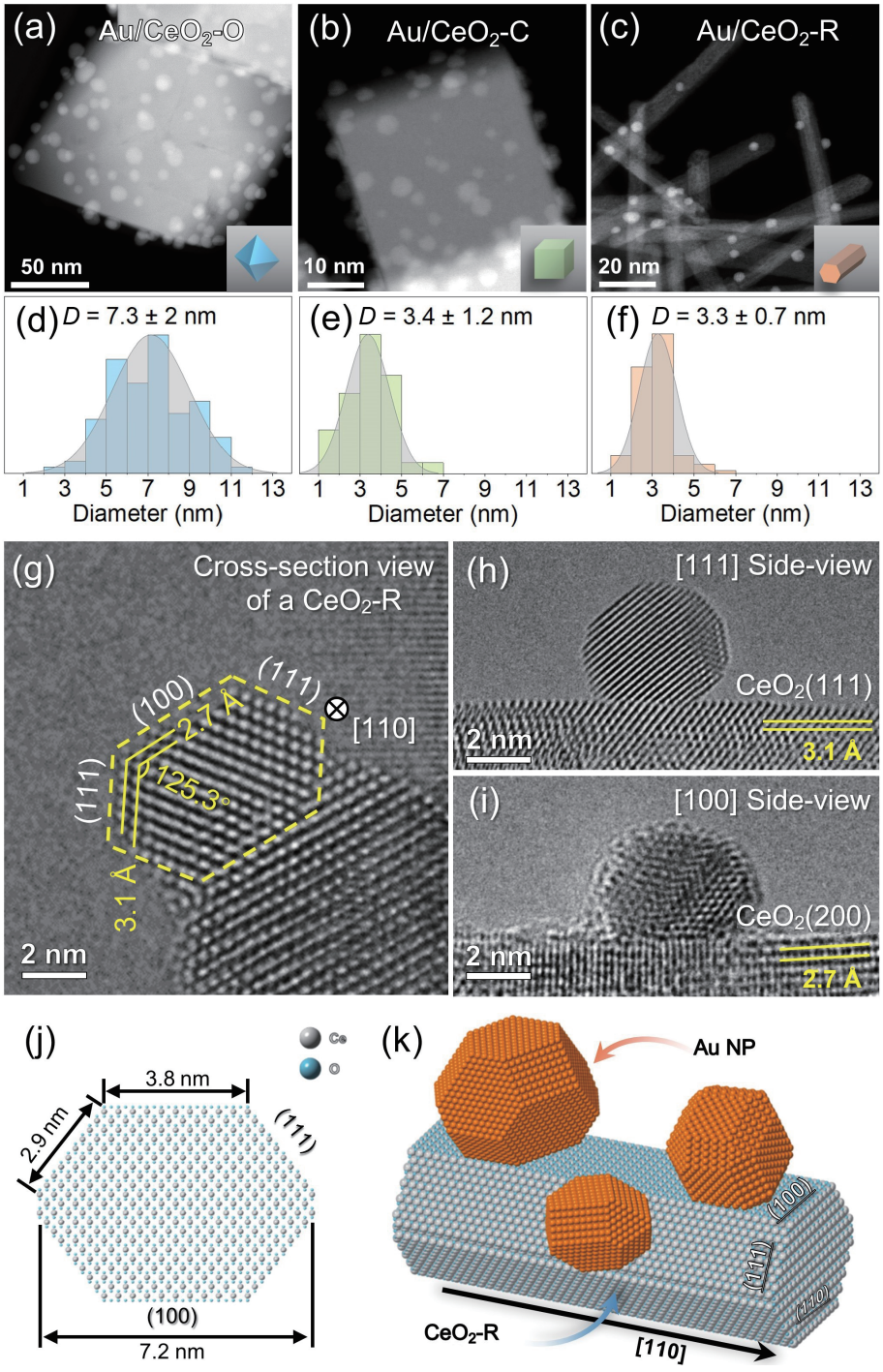

Figure 1 The structure of Au NPs on three CeO_2 supports. ((a)–(f)) HAADF images of the Au/CeO_2-O (a), Au/CeO_2-C (b), and Au/CeO_2-R (c), and corresponding Au NP diameter distributions ((d)–(f)). (g) The cross-sectional view of CeO_2-R along the [110] direction. ((h) and (i)) The perspective views of Au NPs on CeO_2-R(111) (h) and CeO_2-R(200) (i) surfaces. ((j) and (k)) Schematic of a three-dimensional model of CeO_2-R (k) loaded with Au NPs, along with a representation of its cross-section (j).

Au nanoparticles is not thermodynamically favored due to the Ehrlich–Schwoebel (E–S) barrier for the diffusion of Au atoms across the step/edge [53]. This leads to a large chance that the Au nanoparticles located with an "edge-on" position on the CeO_2 substrate, as illustrated in Fig. 2(f). The schematic in Fig. 2(d) shows the common interface on a planar surface of the substrate (noted as "planar-interface") while the case for an "edge-interface" between the Au nanoparticle and the CeO_2 nanorod is shown in Fig. 2(f), which prevails in our Au/CeO_2-R catalysts. The corresponding "planar-interface" and "edge-interface" are highlighted by yellow and red color. This is also illustrated by the atomic image of Fig. 2(d) (more examples are seen in Fig. S7 in the ESM), where Au NPs are in direct contact with the edges of CeO_2-R. The "edge-interface" sites possess distinctive coordination environment and chemical state compared with the common "planar-interface", as shown below.

2.2 Defect structure and adsorption property of the "edge-interface"

The metal–support interface is considered as one of the critical active sites for many catalytic reactions [53]. For CO oxidation, pure CeO_2 exhibits no activity below 200 °C, but after loading Au onto the CeO_2, it shows significant activity at as low as 100 °C [44]. It is generally believed that CeO_2 participates in this reaction through the Mars–van Krevelen (M–vK) mechanism, where the

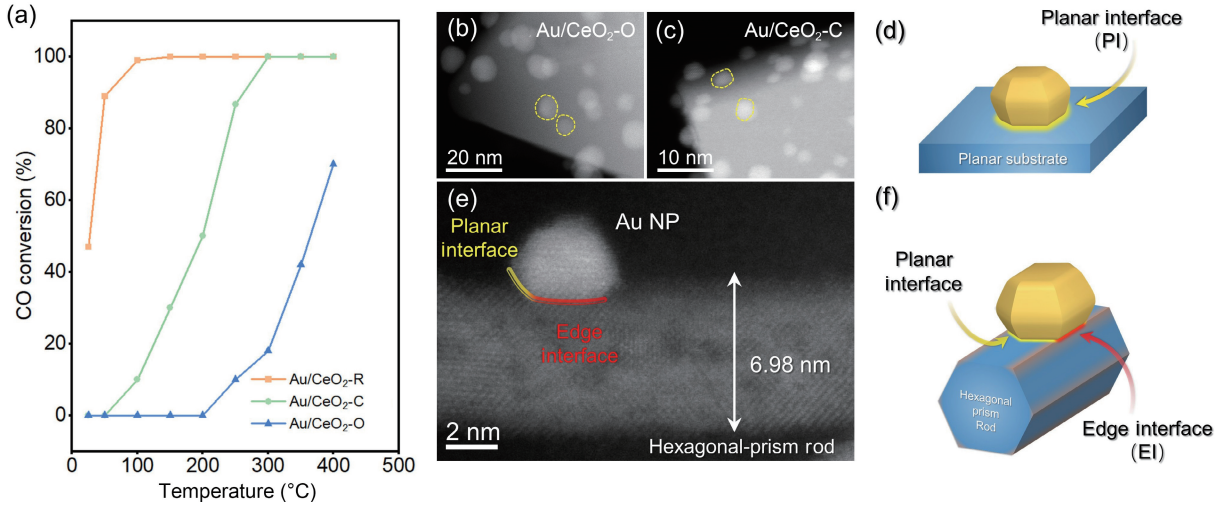

Figure 2 The edge-interface between the Au NPs and CeO_2 support. (a) Catalytic performance of three different Au/CeO_2 catalysts for the CO oxidation reaction. ((b) and (c)) STEM-HAADF images of Au NPs on CeO_2-O (b) and CeO_2-C (c). (d) Schematic of conventional planar-interface between Au NP and CeO_2 substrate. (e) High-magnification HAADF imaging of Au NP loaded on CeO_2-R. (f) Schematic of both planar-interface and edge-interface between Au NP and CeO_2 nanorod substrate.

lattice O reacts with the adsorbed CO to form CO_2 at the Au–CeO_2 interface [23, 24, 54]. The facile dissociative chemisorption of O_2 at the defect sites on CeO_2 provides the source for the lattice O to react with CO, which mainly adsorbed on Au surface.

Thus, we constructed atomic models of pure CeO_2(100) and (111) crystal planes and compared with the edge sites between them, i.e., (100) × (111) and (111) × (111), in terms of the formation energy of OV via DFT calculation. An Au9 cluster was loaded onto the surfaces to investigate the adsorption of CO on the planar and edge-interface sites (see details in the Methods section in the ESM).

According to DFT calculations (Fig. 3(a)), CeO_2(111) surface has the highest OV formation energy of 2.905 eV, followed by the (100) facet of 2.125 eV, which is consistent with previous research findings [53]. For edge-interface sites, OV formation energy of (100) × (111) edge-interface is 1.145 eV, and (111) × (111) edge-interface is 1.455 eV, both of which are much lower than that of planar sites. This implies that the O atoms at the interface are more likely to escape from the lattice and facilitate the O supply during the catalytic reactions. This is similar to the reason of higher reactivity of the (110) crystal plane [39]. We also evaluated the CO adsorption property of the above structure models, which is the first step of the molecular process during the CO oxidation. Through the calculation of the CO adsorption energy at several typical sites on the Au9/CeO_2 model, we can determine the specificity of the edge-interface sites in CO oxidation reaction. As shown in Figs. 3(b)–3(e), the CO adsorption energies of Au at the edge-interface site are −2.49 and −2.09 eV, while the planar site adsorption energy on (100) facet is −1.95 eV and (111) facet is −1.64 eV. These results indicate that CO molecules are more likely to adsorb at the edge-interface sites compared with other planar-interface sites.

Above observations and calculations have revealed an important geometric confinement between Au nanoparticles and the CeO_2 support, noted as the "edge-interface", which is expected to affect the Au/CeO_2 interfacial properties. It's natural that unsaturated coordination and defected atomic structures could affect the adsorption/desorption behaviors of gas molecules and the active sites for specific reaction [54], e.g., CO oxidation, as shown below.

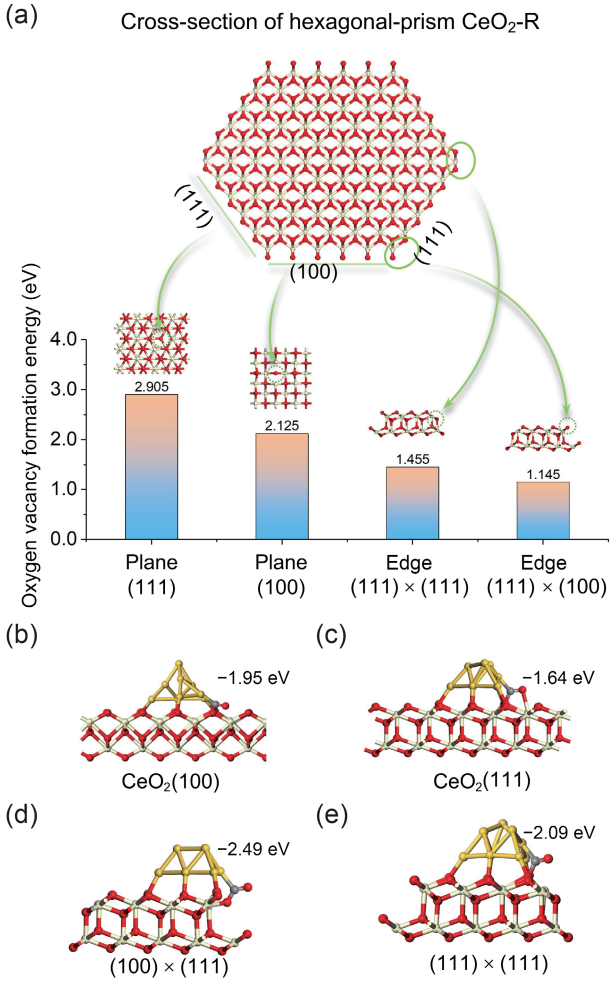

Figure 3 (a) The O vacancy formation energy at typical sites of CeO_2-R. ((b)–(e)) The adsorption energies of CO at various representative sites determined via DFT calculations, interface between Au9 and CeO_2(100) surface (b), and Au9 and CeO_2(111) surface (c), and edge-interface between Au9 and edge (100) × (111) (d), and Au9 and edge (100) × (111) (e).

2.3 CO adsorption behavior at the "edge-interface" by *in situ* DRIFTS

In situ DRIFTS experiments were conducted on three pure CeO_2 supports and corresponding Au/CeO_2 catalysts, as shown in Fig. 4.

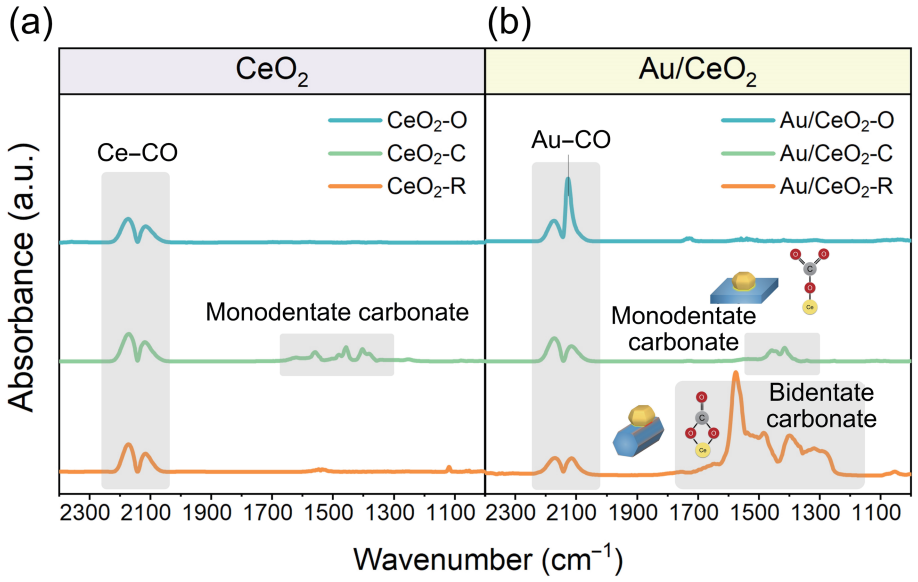

Figure 4 CO DRIFTS investigations of CeO_2 support and Au/CeO_2 catalysts. *In situ* CO DRIFT spectra of CO absorption at 100 °C on (a) pure CeO_2 supports on the left and (b) Au/CeO_2 catalysts on the right.

We focus on CO adsorption and reaction behaviors at a temperature of 100 °C as the performance difference is most pronounced at this temperature.

The region above 2000 cm^{-1} is the linear adsorption region, where Ce–CO absorption is at 2171 and 2117 cm^{-1} [37, 55], Au–CO absorption is at 2115 cm^{-1} [56, 57]. On the CeO_2-O samples (blue line), the loading of Au significantly influences the adsorption of Ce–CO, with the adsorption of Au–CO being significantly higher than that of Ce–CO. On the CeO_2-C samples (green line), there is no significant change of linear absorption sites observed before and after Au loading. This is attributed to the fact that the (111) facet in the CeO_2-O exhibits the weakest CO adsorption ability, while the (100) facet shows relatively strong CO adsorption. Consequently, Au–CO adsorption is strong on the Au/CeO_2-O sample, while Ce–CO adsorption prevails on the Au/CeO_2-C. And for Au/CeO_2-R sample (orange line) which exposes a mixture of both (100) and (111) crystal planes, the proportion of relative strength of Au–CO and Ce–CO linear absorption sites exhibits a degree of magnitude that lies between the above two morphologies.

For the CO adsorption on Au/CeO_2 catalysts, aside from linear adsorption sites, CO also interacts with CeO_2 surface to form carbonate species, which provides direct insights to CO oxidation reaction through lattice O route (M–vK mechanism). The Au/CeO_2-R sample shows distinct CO adsorption behaviors with both the Au/CeO_2-O and Au/CeO_2-C samples. On the sample of either CeO_2-O support or Au/CeO_2-O catalyst, no carbonate species has ever been detected; on both CeO_2-C support and Au/CeO_2-C catalyst samples, peaks of monodentate carbonates [55, 58, 59] (at 1416 and 1458 cm^{-1}) with similar strength were observed. This is due to that the formation energy of oxygen vacancies on CeO_2(111) surface is large, hindering the formation of carbonate species. On the contrary, the CeO_2(100) surface is smaller, leading to the formation of monodentate carbonates in the CeO_2-C support. And after Au loading, the negligible change in intensity of the carbonate species peak suggests that the Au-CeO_2(100) interface does not affect the carbonate formation under this condition. For the carbonate formation of rod-shaped samples, there is almost no carbonate signal on pure CeO_2-R support, however, when Au is loaded onto rods, a large amount of bidentate carbonates [55, 58, 59] (at 1576 and 1292 cm^{-1}) signals were detected, indicating that the large amount of edge-interface sites enhance the interaction between CO and CeO_2, which facilitates the CO oxidation reaction through the lattice O route, resulting from the variations in the amount and species of adsorbed carbonates.

2.4 Quantification of the "edge-interface" of Au/CeO_2-R catalysts

After demonstrating the surface properties of the "edge-interface", we attempt to evaluate this unique interfacial structure quantitatively. We synthesized two rod-shaped Au/CeO_2 catalysts with different CeO_2 nanorods with sizes of 12.7 ± 1.4 nm (CeO_2-R12) vs. 7.6 ± 1.5 nm (CeO_2-R7) in order to control the number of edge-interface sites for the Au/CeO_2-R catalyst. The size of Au nanoparticles with a diameter of ~ 3 nm was controlled using the direct solvated-metal-nanoparticle-dispersion method to eliminate the influence of further particle growth during the preparation process. The morphology and size of Au/CeO_2-R catalysts were confirmed by scanning transmission electron microscopy (STEM)-HAADF, as shown in Figs. 5(a) and 5(b) (more shown in Fig. S8 in the ESM). The difference in the particle size of Au is negligible, and we can observe that the Au/CeO_2-R12 has fewer edge-interface sites compared with Au/CeO_2-R7 catalyst due to its larger surface area. If we keep the same size and the density of Au nanoparticles for two catalysts with a presumed uniform distribution of Au, we can calculate that the number of edge-interface sites in CeO_2-R7 sample is much larger than that in CeO_2-R12 (see details in the ESM).

The XPS results in Fig. 5(c) demonstrate that there is no difference in Ce 3d and O 1s for these two samples, implying that CeO_2-R7 and CeO_2-R12 have the same intrinsic surface properties such as the defected surface and the number of O vacancies. However, the Au on CeO_2-R7 shows a higher proportion of Au^{3+} compared with Au/CeO_2-R12. The increasing amount of Au^{3+} is a sign that the Au particles share an edge with the CeO_2 hexagonal prism, and induce a stronger charge transfer between Au and CeO_2 compared with the regular Au/CeO_2 planar-interface sites, leading to a higher oxidation state of Au as observed here [60]. Besides, we also conducted XPS testing on both the Au/CeO_2-O and Au/CeO_2-C samples, and we found that no evidence of Au^{3+} in these samples inferring the existence of Au^{3+} is more popular for the sample with the edge interface, as shown in Fig. S9 in the ESM. From *in situ* CO DRIFTS results shown in Fig. 5(d), despite the peak shift being observed in carbonate species with temperature rising, we can still demonstrate that the Au/CeO_2-R7 exhibits a higher intensity of peaks for bidentate carbonate species

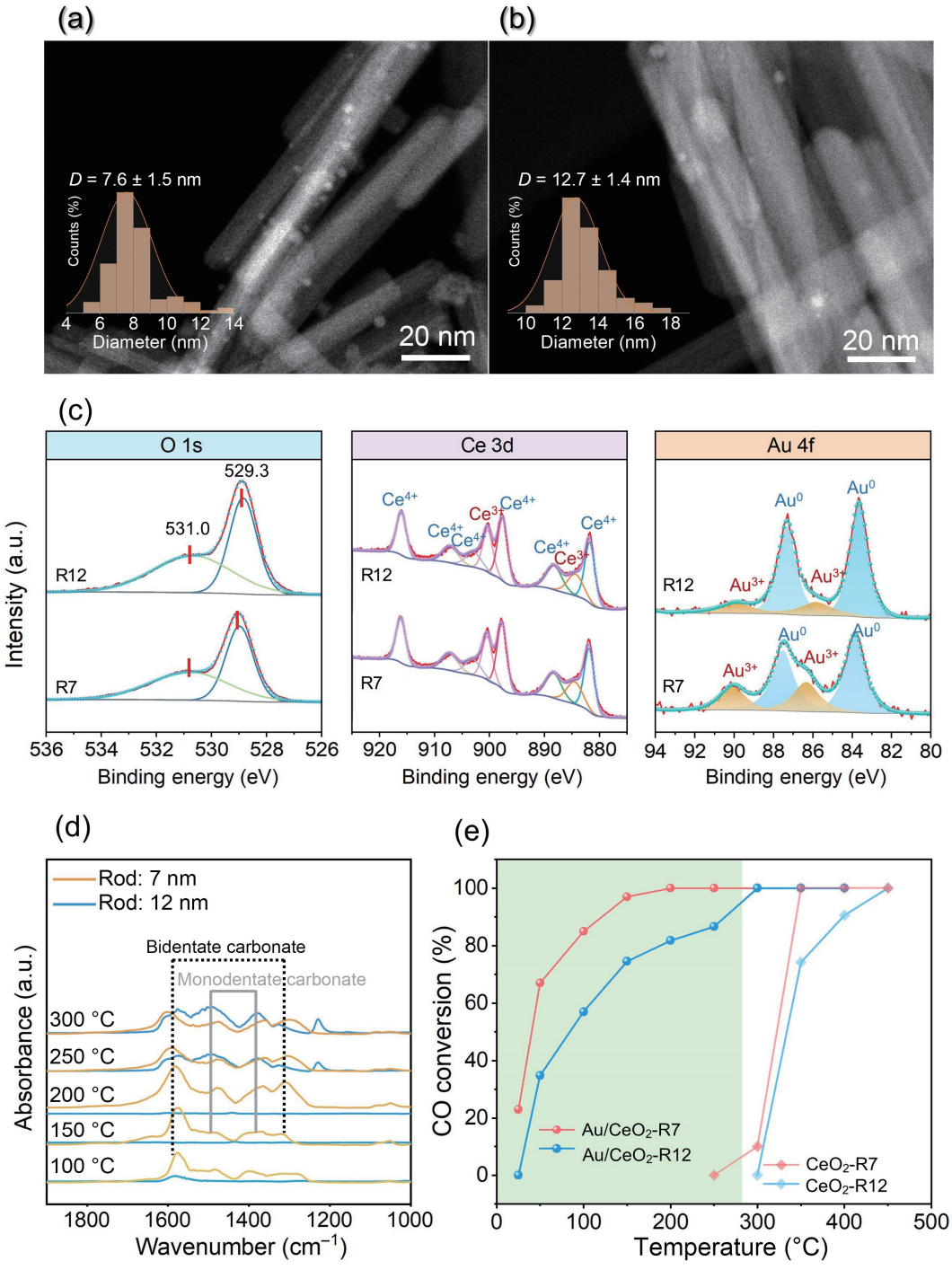

Figure 5 The edge-interface dependent Au/CeO_2-R catalysts for CO oxidation performance. ((a) and (b)) STEM-HAADF images and size distribution of CeO_2-R7 (a) and CeO_2-R12 (b). (c) XPS spectra of O 1s, Ce 3d, and Au 4f of Au/CeO_2-R catalysts. (d) *In situ* CO DRIFTS analysis of two Au/CeO_2-R catalysts. (e) Catalytic activities of Au/CeO_2-R7, Au/CeO_2-R12, CeO_2-R7, and CeO_2-R12.

throughout the entire temperature range compared with Au/CeO_2-R12, indicating that the edge-interface sites serve as a bidentate adsorption site, and will contribute to the CO oxidation reaction as shown below.

The performance testing was conducted on both pure CeO_2-R supports and Au/CeO_2-R catalysts, as shown in Fig. 5(e). The Au loading amount of ~ 5 wt.% in Au/CeO_2 catalysts was determined by inductively coupled plasma (ICP) analysis (Table S1 in the ESM). The Au/CeO_2-R7 catalyzed the CO oxidation reaction at a lower temperature and exhibited a higher CO conversion rate than Au/CeO_2-R12 catalyst for the whole temperature range, while the pure CeO_2 supports did not show any performance below 300 °C, indicating that the disparities in performance are independent of differences in CeO_2 support itself at this temperature range. This comparison clearly demonstrates an enhancement in catalytic performance of Au/CeO_2-R with the increasing "edge-interface" sites.

3 Conclusions

In conclusion, we investigated the interfacial structure and property of Au/CeO_2 catalysts with different morphologies of CeO_2 support (cube, octahedron, and nanorod) in details through atomic-scale electron microscopy and revealed a geometric confinement noted as "edge-interface" for the nanorod CeO_2 support, which was not discussed previously. This "edge-interface" features a shared edge between metal nanoparticle and oxide support, thus introducing additional structural freedom to the system. Its defected atomic structure exposes as an active catalytic

surface with an unsaturated coordination environment, which has a lowered formation energy for O vacancy and stronger CO adsorption corroborated by DFT calculation and *in situ* CO DRIFTS analysis. We further tested the Au/CeO_2-R catalysts with varied "edge-interface" sites and found an "edge-interface" dependent CO conversion rate. These results enrich the fundamental understanding of metal/oxide interfacial structure and property by providing precise structure–performance correlation, and also provide strategies to maximize the effective active sites for heterogeneous catalysis.

Acknowledgements

The authors appreciate the support from the National Natural Science Foundation of China (Nos. 22172110 and 12364018) and the Guangxi Science and Technology Major Program (No. AA23073019). We thank the Haihe Laboratory of Sustainable Chemical Transformations for financial support. We thank the Facility Center at the Institute of Molecular Plus at Tianjin University, Facility and Analysis Center at Guangxi University, and Electron Microscopy Center at the Dalian Institute of Chemical Physics, Chinese Academy of Sciences to use the transmission electron microscopy.

Electronic Supplementary Material: Supplementary material (detailed experimental procedures, calculation methods, XRD patterns, STEM images, EDS maps, HRTEM images, and ICP-optical emission spectroscopy (OES) results) is available in the online version of this article at https://doi.org/10.1007/s12274-024-6508-6.

References

[1] Sankar, M.; He, Q.; Engel, R. V.; Sainna, M. A.; Logsdail, A. J.; Roldan, A.; Willock, D. J.; Agarwal, N.; Kiely, C. J.; Hutchings, G. J. Role of the support in gold-containing nanoparticles as heterogeneous catalysts. *Chem. Rev.* **2020**, *120*, 3890–3938.

[2] Li, Z.; Ji, S. F.; Liu, Y. W.; Cao, X.; Tian, S. B.; Chen, Y. J.; Niu, Z. Q.; Li, Y. D. Well-defined materials for heterogeneous catalysis: From nanoparticles to isolated single-atom sites. *Chem. Rev.* **2020**, *120*, 623–682.

[3] van Deelen, T. W.; Hernández Mejía, C.; de Jong, K. P. Control of metal–support interactions in heterogeneous catalysts to enhance activity and selectivity. *Nat. Catal.* **2019**, *2*, 955–970.

[4] Liu, L. C.; Corma, A. Metal catalysts for heterogeneous catalysis: From single atoms to nanoclusters and nanoparticles. *Chem. Rev.* **2018**, *118*, 4981–5079.

[5] Munnik, P.; de Jongh, P. E.; de Jong, K. P. Recent developments in the synthesis of supported catalysts. *Chem. Rev.* **2015**, *115*, 6687–6718.

[6] Ta, N.; Liu, J. Y.; Chenna, S.; Crozier, P. A.; Li, Y.; Chen, A. L.; Shen, W. J. Stabilized gold nanoparticles on ceria nanorods by strong interfacial anchoring. *J. Am. Chem. Soc.* **2012**, *134*, 20585–20588.

[7] Wang, Y. C.; Widmann, D.; Behm, R. J. Influence of TiO_2 bulk defects on CO adsorption and CO oxidation on Au/TiO_2: Electronic metal–support interactions (EMSIs) in supported Au catalysts. *ACS Catal.* **2017**, *7*, 2339–2345.

[8] Carrettin, S.; Concepción, P.; Corma, A.; López Nieto, J. M.; Puntes, V. F. Nanocrystalline CeO_2 increases the activity of Au for CO oxidation by two orders of magnitude. *Angew. Chem., Int. Ed.* **2004**, *43*, 2538–2540.

[9] Fu, Q.; Saltsburg, H.; Flytzani-Stephanopoulos, M. Active nonmetallic Au and Pt species on ceria-based water–gas shift catalysts. *Science* **2003**, *301*, 935–938.

[10] Sakurai, H.; Ueda, A.; Kobayashi, T.; Haruta, M. Low-temperature water–gas shift reaction over gold deposited on TiO_2. *Chem. Commun*. **1997**, 271–272.

[11] Yuan, W. T.; Zhu, B. E.; Fang, K.; Li, X. Y.; Hansen, T. W.; Ou, Y.; Yang, H. S.; Wagner, J. B.; Gao, Y.; Wang, Y. et al. *In situ* manipulation of the active Au-TiO_2 interface with atomic precision during CO oxidation. *Science* **2021**, *371*, 517–521.

[12] Suchorski, Y.; Kozlov, S. M.; Bespalov, I.; Datler, M.; Vogel, D.; Budinska, Z.; Neyman, K. M.; Rupprechter, G. The role of metal/oxide interfaces for long-range metal particle activation during CO oxidation. *Nat. Mater.* **2018**, *17*, 519–522.

[13] Ha, H.; Yoon, S.; An, K.; Kim, H. Y. Catalytic CO oxidation over Au nanoparticles supported on CeO_2 nanocrystals: Effect of the Au–CeO_2 interface. *ACS Catal.* **2018**, *8*, 11491–11501.

[14] Saavedra, J.; Doan, H. A.; Pursell, C. J.; Grabow, L. C.; Chandler, B. D. The critical role of water at the gold–titania interface in catalytic CO oxidation. *Science* **2014**, *345*, 1599–1602.

[15] Cargnello, M.; Doan-Nguyen, V. V. T.; Gordon, T. R.; Diaz, R. E.; Stach, E. A.; Gorte, R. J.; Fornasiero, P.; Murray, C. B. Control of metal nanocrystal size reveals metal–support interface role for ceria catalysts. *Science* **2013**, *341*, 771–773.

[16] Ahn, S. Y.; Jang, W. J.; Shim, J. O.; Jeon, B. H.; Roh, H. S. CeO_2-based oxygen storage capacity materials in environmental and energy catalysis for carbon neutrality: Extended application and key catalytic properties. *Catal. Rev.*, in press, https://doi.org/10.1080/01614940.2022.2162677.

[17] Liu, J. C.; Luo, L. L.; Xiao, H.; Zhu, J. F.; He, Y.; Li, J. Metal affinity of support dictates sintering of gold catalysts. *J. Am. Chem. Soc.* **2022**, *144*, 20601–20609.

[18] Zhang, Y.; Zhao, S. N.; Feng, J.; Song, S. Y.; Shi, W. D.; Wang, D.; Zhang, H. J. Unraveling the physical chemistry and materials science of CeO_2-based nanostructures. *Chem* **2021**, *7*, 2022–2059.

[19] He, Y.; Liu, J. C.; Luo, L. L.; Wang, Y. G.; Zhu, J. F.; Du, Y. G.; Li, J.; Mao, S. X.; Wang, C. M. Size-dependent dynamic structures of supported gold nanoparticles in CO oxidation reaction condition. *Proc. Natl. Acad. Sci. USA* **2018**, *115*, 7700–7705.

[20] Rodriguez, J. A.; Grinter, D. C.; Liu, Z. Y.; Palomino, R. M.; Senanayake, S. D. Ceria-based model catalysts: Fundamental studies on the importance of the metal–ceria interface in CO oxidation, the water-gas shift, CO_2 hydrogenation, and methane and alcohol reforming. *Chem. Soc. Rev.* **2017**, *46*, 1824–1841.

[21] Luo, L. L.; Chen, S. Y.; Xu, Q.; He, Y.; Dong, Z. J.; Zhang, L. F.; Zhu, J. F.; Du, Y. G.; Yang, B.; Wang, C. M. Dynamic atom clusters on AuCu nanoparticle surface during CO oxidation. *J. Am. Chem. Soc.* **2020**, *142*, 4022–4027.

[22] Chang, M. W.; Zhang, L.; Davids, M.; Filot, I. A. W.; Hensen, E. J. M. Dynamics of gold clusters on ceria during CO oxidation. *J. Catal.* **2020**, *392*, 39–47.

[23] Kim, H. Y.; Lee, H. M.; Henkelman, G. CO oxidation mechanism on CeO_2-supported Au nanoparticles. *J. Am. Chem. Soc.* **2012**, *134*, 1560–1570.

[24] Guzman, J.; Carrettin, S.; Corma, A. Spectroscopic evidence for the supply of reactive oxygen during CO oxidation catalyzed by gold supported on nanocrystalline CeO_2. *J. Am. Chem. Soc.* **2005**, *127*, 3286–3287.

[25] Soler, L.; Casanovas, A.; Urrich, A.; Angurell, I.; Llorca, J. CO oxidation and COPrOx over preformed Au nanoparticles supported over nanoshaped CeO_2. *Appl. Catal. B: Environ.* **2016**, *197*, 47–55.

[26] Reina, T. R.; Ivanova, S.; Laguna, O. H.; Centeno, M. A.; Odriozola, J. A. WGS and CO-PrO_x reactions using gold promoted copper-ceria catalysts: "Bulk CuO-CeO_2 vs. CuO-CeO2/Al_2O_3 with low mixed oxide content". *Appl. Catal. B: Environ.* **2016**, *197*, 62–72.

[27] Pozdnyakova, O.; Teschner, D.; Wootsch, A.; Kröhnert, J.; Steinhauer, B.; Sauer, H.; Toth, L.; Jentoft, F. C.; Knop-Gericke, A.; Paál, Z. et al. Preferential CO oxidation in hydrogen (PROX) on ceria-supported catalysts, part I: Oxidation state and surface species on Pt/CeO_2 under reaction conditions. *J. Catal.* **2006**, *237*, 1–16.

[28] Ning, J.; Zhou, Y.; Shen, W. J. Atomically dispersed copper species on ceria for the low-temperature water–gas shift reaction. *Sci. China Chem.* **2021**, *64*, 1103–1110.

[29] Karpenko, A.; Leppelt, R.; Cai, J.; Plzak, V.; Chuvilin, A.; Kaiser, U.; Behm, R. J. Deactivation of a Au/CeO_2 catalyst during the low-temperature water–gas shift reaction and its reactivation: A combined TEM, XRD, XPS, DRIFTS, and activity study. *J. Catal.* **2007**, *250*, 139–150.

[30] Fu, Q.; Kudriavtseva, S.; Saltsburg, H.; Flytzani-Stephanopoulos, M. Gold-ceria catalysts for low-temperature water–gas shift reaction. *Chem. Eng. J.* **2003**, *93*, 41–53.
[31] Li, Y. Y.; Kottwitz, M.; Vincent, J. L.; Enright, M. J.; Liu, Z. Y.; Zhang, L. H.; Huang, J. H.; Senanayake, S. D.; Yang, W. C. D.; Crozier, P. A. et al. Dynamic structure of active sites in ceria-supported Pt catalysts for the water gas shift reaction. *Nat. Commun.* **2021**, *12*, 914.
[32] Andreeva, D.; Idakiev, V.; Tabakova, T.; Ilieva, L.; Falaras, P.; Bourlinos, A.; Travlos, A. Low-temperature water–gas shift reaction over Au/CeO_2 catalysts. *Catal. Today* **2002**, *72*, 51–57.
[33] Wen, Y.; Huang, Q. Y.; Zhang, Z. H.; Huang, W. X. Morphology-dependent catalysis of CeO_2-based nanocrystal model catalysts. *Chin. J. Chem.* **2022**, *40*, 1856–1866.
[34] Lin, Y. Y.; Wu, Z. L.; Wen, J. G.; Ding, K. L.; Yang, X. Y.; Poeppelmeier, K. R.; Marks, L. D. Adhesion and atomic structures of gold on ceria nanostructures: The role of surface structure and oxidation state of ceria supports. *Nano Lett.* **2015**, *15*, 5375–5381.
[35] Li, Y.; Shen, W. J. Morphology-dependent nanocatalysts: Rod-shaped oxides. *Chem. Soc. Rev.* **2014**, *43*, 1543–1574.
[36] Huang, W. X.; Gao, Y. X. Morphology-dependent surface chemistry and catalysis of CeO_2 nanocrystals. *Catal. Sci. Technol.* **2014**, *4*, 3772–3784.
[37] Wu, Z. L.; Li, M. J.; Overbury, S. H. On the structure dependence of CO oxidation over CeO_2 nanocrystals with well-defined surface planes. *J. Catal.* **2012**, *285*, 61–73.
[38] Tana; Zhang, M. L.; Li, J.; Li, H. J.; Li, Y.; Shen, W. J. Morphology-dependent redox and catalytic properties of CeO_2 nanostructures: Nanowires, nanorods and nanoparticles. *Catal. Today* **2009**, *148*, 179–183.
[39] Zhou, K.; Wang, X.; Sun, X. M.; Peng, Q.; Li, Y. D. Enhanced catalytic activity of ceria nanorods from well-defined reactive crystal planes. *J. Catal.* **2005**, *229*, 206–212.
[40] Aneggi, E.; Llorca, J.; Boaro, M.; Trovarelli, A. Surface-structure sensitivity of CO oxidation over polycrystalline ceria powders. *J. Catal.* **2005**, *234*, 88–95.
[41] Zhang, L. J.; Chen, R. H.; Tu, Y.; Gong, X. Y.; Cao, X.; Xu, Q.; Li, Y.; Ye, B. J.; Ye, Y. F.; Zhu, J. F. Revealing the crystal facet effect of ceria in Pd/CeO_2 catalysts toward the selective oxidation of benzyl alcohol. *ACS Catal.* **2023**, *13*, 2202–2213.
[42] Li, Z. M.; Zhang, X. Y.; Shi, Q. Q.; Gong, X.; Xu, H.; Li, G. Morphology effect of ceria supports on gold nanocluster catalyzed CO oxidation. *Nanoscale Adv.* **2021**, *3*, 7002–7006.
[43] Jiang, F.; Wang, S. S.; Liu, B.; Liu, J.; Wang, L.; Xiao, Y.; Xu, Y. B.; Liu, X. H. Insights into the influence of CeO_2 crystal facet on CO_2 hydrogenation to methanol over Pd/CeO_2 catalysts. *ACS Catal.* **2020**, *10*, 11493–11509.
[44] Huang, X. S.; Sun, H.; Wang, L. C.; Liu, Y. M.; Fan, K. N.; Cao, Y. Morphology effects of nanoscale ceria on the activity of Au/CeO_2 catalysts for low-temperature CO oxidation. *Appl. Catal. B: Environ.* **2009**, *90*, 224–232.
[45] Mai, H. X.; Sun, L. D.; Zhang, Y. W.; Si, R.; Feng, W.; Zhang, H. P.; Liu, H. C.; Yan, C. H. Shape-selective synthesis and oxygen storage behavior of ceria nanopolyhedra, nanorods, and nanocubes. *J. Phys. Chem. B* **2005**, *109*, 24380–24385.
[46] Si, R.; Flytzani-Stephanopoulos, M. Shape and crystal-plane effects of nanoscale ceria on the activity of Au-CeO_2 catalysts for the water-gas shift reaction. *Angew. Chem., Int. Ed.* **2008**, *47*, 2884–2887.
[47] Nolan, M.; Watson, G. W. The surface dependence of CO adsorption on ceria. *J. Phys. Chem. B* **2006**, *110*, 16600–16606.
[48] Nolan, M.; Parker, S. C.; Watson, G. W. The electronic structure of oxygen vacancy defects at the low index surfaces of ceria. *Surf. Sci.* **2005**, *595*, 223–232.
[49] Liu, X. W.; Zhou, K. B.; Wang, L.; Wang, B. Y.; Li, Y. D. Oxygen vacancy clusters promoting reducibility and activity of ceria nanorods. *J. Am. Chem. Soc.* **2009**, *131*, 3140–3141.
[50] Trovarelli, A.; Llorca, J. Ceria catalysts at nanoscale: How do crystal shapes shape catalysis. *ACS Catal.* **2017**, *7*, 4716–4735.
[51] Yao, S. Y.; Xu, W. Q.; Johnston-Peck, A. C.; Zhao, F. Z.; Liu, Z. Y.; Luo, S.; Senanayake, S. D.; Martínez-Arias, A.; Liu, W. J.; Rodriguez, J. A. Morphological effects of the nanostructured ceria support on the activity and stability of CuO/CeO_2 catalysts for the water–gas shift reaction. *Phys. Chem. Chem. Phys.* **2014**, *16*, 17183–17195.
[52] Zanella, R.; Giorgio, S.; Henry, C. R.; Louis, C. Alternative methods for the preparation of gold nanoparticles supported on TiO_2. *J. Phys. Chem. B* **2002**, *106*, 7634–7642.
[53] Haftel, M. I. Ehrlich–Schwoebel effect for vacancies: Low-index faces of silver. *Phys. Rev. B* **2001**, *64*, 125415.
[54] Kim, H. Y.; Henkelman, G. CO oxidation at the interface of Au nanoclusters and the stepped-CeO_2 (111) surface by the Mars–van Krevelen mechanism. *J. Phys. Chem. Lett.* **2013**, *4*, 216–221.
[55] Li, C.; Sakata, Y.; Arai, T.; Domen, K.; Maruya, K. I.; Onishi, T. Carbon monoxide and carbon dioxide adsorption on cerium oxide studied by Fourier-transform infrared spectroscopy. Part 1. Formation of carbonate species on dehydroxylated CeO_2, at room temperature. *J. Chem. Soc., Faraday Trans. 1: Phys. Chem. Condens. Phases* **1989**, *85*, 929–943.
[56] Fu, X. P.; Guo, L. W.; Wang, W. W.; Ma, C.; Jia, C. J.; Wu, K.; Si, R.; Sun, L. D.; Yan, C. H. Direct identification of active surface species for the water–gas shift reaction on a gold-ceria catalyst. *J. Am. Chem. Soc.* **2019**, *141*, 4613–4623.
[57] Jin, Z.; Song, Y. Y.; Fu, X. P.; Song, Q. S.; Jia, C. J. Nanoceria supported gold catalysts for CO oxidation. *Chin. J. Chem.* **2018**, *36*, 639–643.
[58] Chen, S. L.; Luo, L. F.; Jiang, Z. Q.; Huang, W. X. Size-dependent reaction pathways of low-temperature CO oxidation on Au/CeO_2 catalysts. *ACS Catal.* **2015**, *5*, 1653–1662.
[59] Vayssilov, G. N.; Mihaylov, M.; Petkov, P. S.; Hadjiivanov, K. I.; Neyman, K. M. Reassignment of the vibrational spectra of carbonates, formates, and related surface species on ceria: A combined density functional and infrared spectroscopy investigation. *J. Phys. Chem. C* **2011**, *115*, 23435–23454.
[60] Camellone, M. F.; Fabris, S. Reaction mechanisms for the CO oxidation on Au/CeO_2 catalysts: Activity of substitutional Au^{3+}/Au^{+} cations and deactivation of supported Au^{+} adatoms. *J. Am. Chem. Soc.* **2009**, *131*, 10473–10483.